This article has been accepted for publication in a future issue of this journal, but has not been fully edited. Content may change prior to final publication. Citation information: DOI 10.1109/TMI.2017.2777891, IEEE Transactions on Medical Imaging

Importance of ultrawide bandwidth for optoacoustic esophagus imaging

Hailong He, *Graduate Student Member, IEEE,* Andreas Buehler, Dmitry Bozhko, Xiaohua Jian,

Yaoyao Cui and Vasilis Ntziachristos*, *Senior Member, IEEE*

***Abstract*— Optoacoustic (photoacoustic) endoscopy has shown potential to reveal complementary contrast to optical endoscopy methods, indicating clinical relevance. However operational parameters for accurate optoacoustic endoscopy must be specified for optimal performance. Recent support from the EU Horizon 2020 program ESOTRAC to develop a next-generation optoacoustic esophageal endoscope directs the interrogation of the optimal frequency required for accurate implementation. We simulated the frequency response of the esophagus wall and then validated the simulation results with experimental measurements of pig esophagus. Phantoms and fresh pig esophagus samples were measured using two detectors with central frequencies of 15 or 50 MHz, and the imaging performance of both detectors was compared. We analyzed the frequency bandwidth of optoacoustic signals in relation to morphological layer structures of the esophagus and found the 50 MHz detector to differentiate layer structures better than the 15 MHz detector. Furthermore, we identify the necessary detection bandwidth for visualizing esophagus morphology and selecting ultrasound transducers for future optoacoustic endoscopy of the esophagus.**

***Index Terms*— Photoacoustic imaging, optoacoustic imaging, esophagus imaging, ultrawide bandwidth**

I. Introduction

Earlier detection of esophageal cancer closely relates to improved prognosis and healthcare costs savings. However, even with regular surveillance, the current imaging standard based on white light endoscopy (WLE) has miss-rates reaching ~57% [1, 2]. Moreover, staging of esophageal cancer depends on the depth of the infiltration and the extent of damage to histological layers of the esophageal wall, which is not assessed by WLE [3-5]. Ultrasound endoscopy is a widely used clinical imaging modality in esophageal cancer staging to provide high-speed and high-resolution cross-sectional imaging over a large field of view [6]. However, poor tissue contrast limits the ability of ultrasound endoscopy to identify superficial layer structures, resulting in low accuracy of earlier esophageal cancer staging [7]. Recently developed optical endoscopic imaging modalities, such as endoscopic optical coherence tomography [8, 9] and confocal endoscopy [10], have shown promise for improving disease detection and identifying dysplasia. Confocal endoscopy nevertheless is limited to inspecting small fields of view at a time, and it is not well suited for surveillance of the entire esophageal wall. OCT offers a better outlook for inspecting the entire organ but reveals only morphological contrast, possibly missing pathophysiological characterization of the disease.

Optoacoustic endoscopy has been considered as an alternative endoscopy technique, which is administered analogously to OCT but allows visualization of hemodynamic and molecular contrast [11-13]. In addition, optoacoustics can penetrate deeper than OCT, possibly allowing more comprehensive staging. Optoacoustic imaging is insensitive to photon scattering within biological tissues, providing high-resolution optical visualization deeper in tissue than conventional optical imaging methods [14, 15]. Multispectral optoacoustic methods have been widely applied to resolve vascular structures and tumor hypoxia, as well as the biodistribution of targeted photo-absorbing agents or circulating particles [16, 17]. Optoacoustic endoscopy has been shown to resolve the superficial vascular structure of the esophageal lumen of rats and rabbits [11, 12, 18, 19]. For example, the gastrointestinal tract of a rat and rabbits were imaged in-vivo using a 3.8 mm in diameter optoacoustic imaging probe comprising an integrated light guiding optical fiber, an ultrasonic detector and a mechanical rotating acoustic and optical reflector for sectorial B-scan imaging. Recent implementations of the system feature an additional size reduction to 2.5 mm to fit through the working channel of a standard colonoscope for endoscopic guidance [11, 12, 18, 19]. However, imaging of human or pig esophageal lumen has not yet been investigated. The layer thickness of the mucosa and submucosa in the human esophageal wall varies from a few hundred μm to millimeters, which is markedly greater than the thickness of rat and rabbit esophageal wall, possibly requiring different operational characteristics in terms of detected bandwidth. In our previous work, we investigated ultra-broadband optoacoustic for human skin imaging [20, 21]. Similar to skin, blood vessels in different

This work was supported by the European Union project FAMOS (FP7 ICT, Contract 317744). This project has received funding from the European Union's Horizon 2020 research and innovation programme under grant agreement No 732720 (ESOTRAC). H. He acknowledges support from China Scholarship Council (CSC) Scholarship.

H. He, A. Buehler, D. Bozhko and V. Ntziachristos are with the Chair for Biological Imaging, Technische Universität München, and Institute for Biological and Medical Imaging, Helmholtz Zentrum Munich, Ingolstadter, Landstraße 1, 85764 Neuherberg, Germany. X. Jian and Y. Cui are with Suzhou Institute of Biomedical Engineering and Technology, Chinese Academy of Sciences, NO.88, Keling Road, Suzhou New District, Suzhou, Jiangsu, China. 215163. *e-mail: v.ntziachristos@tum.de.

This article has been accepted for publication in a future issue of this journal, but has not been fully edited. Content may change prior to final publication. Citation information: DOI 10.1109/TMI.2017.2777891, IEEE Transactions on Medical Imaging

layers of esophageal wall range from thin capillaries with a diameter of several μm located in the lamina propria layer to larger vessels with a diameter of up to a hundred μm in deep layers [22]. Thus, the frequency content of optoacoustic signals generated in the esophagus wall is intrinsically broadband and the necessary bandwidth of optoacoustic is required to further investigate for esophageal imaging.

In this study, we interrogated the frequency bandwidth that is best suited for human esophageal imaging. This investigation relates to the selection of a transducer for developing an optoacoustic endoscope for human studies. First, we performed simulations to explore the frequency response of different layer structures in the esophagus wall. Then, we built two optoacoustic endoscopy probes based on intravascular ultrasound (IVUS) transducers with central frequencies of 15 and 50 MHz respectively to measure pig esophageal samples as the histological structure of the pig esophageal wall is similar to that of humans. Images acquired with the two transducers were analyzed to identify the frequency contributions of different layers in the esophageal wall. We summarize our findings and discuss the implications in the selection of components for esophageal optoacoustic endoscopy.

II. Materials and Methods

A. Simulations

To understand the requirements needed for optoacoustic imaging of the esophageal wall, we simulated the optoacoustic response of absorbers in different layers of the wall. Fig. 2(a) illustrates the layers that make up the esophageal wall of humans and other large animals such as pigs: the mucosa (M) comprises epithelium (EP), lamina propria, and muscularis mucosa (MM), followed by the submucosa (SM) and muscularis propria (MP) [22]. The EP layer comprises a layer of cells, while the LP layer is rich in capillaries and lymph vessels with diameters of approximately 10-20 μm [22]. The MM layer is composed mainly of several thin layers of smooth muscle fibers, while the SM contains blood vessels and lymphatic vessels with diameters of 30-50 μm [22]. The thick MP layer comprises muscle fibers and blood vessels with diameters up to 100 μm [22].

Simulations included the layers enriched with blood vessels (LP, SM and MP), and frequency responses were calculated assuming vessels with a diameter of 10 μm in the LP layer, diameters of 30 and 50 μm in the SM layer and 100 μm in the MP layer. Optoacoustic signal was simulated using the analytical solution of the pressure wave equation for a homogeneous spherical absorber with radius a positioned at r_s[23]:

$$p_\delta(r,t) = p_0 U(a - |R - v_s t|)\frac{(R - v_s t)}{2R} \quad (1)$$

where U is the Heaviside function, R is the distance of the absorber from the detection position, p_0 is the amplitude of the initial pressure wave and v_s is the speed of sound. Four spheres with radius a = 5, 15, 25, and 50 μm were simulated. The duration of the simulated pulse correlates with the propagation time of sound along the sphere diameter, and so it scales with sphere size. Fast Fourier transformation of each simulated optoacoustic signal gave the theoretical frequency response$F_t(\mathrm{f},\mathrm{z})$, which is a function of frequency at different depth z. However, acoustic attenuation significantly reduced the high frequency acoustic signals [21, 24]. For the endoscopy imaging configurations, the acoustic attenuation $F_a(f,z)$ is approximated as follows [21, 24]:

$$F_a(f,z) = \exp\left[-z_1 \frac{0.00217dB}{MHz^2 cm} f^2\right] \cdot \exp\left[-z_2 \frac{0.5dB}{MHz\ cm}|f|\right] \quad (2)$$

Where z_1 are the distances between the tissue surfaces to the transducer surface inside water, which approximately equal the near field length of both transducers in all experiments. z_2 are the depths of absorbers inside the soft tissue. The simulations did not take into account the amplitude attenuation in the acoustic attenuation procedure. Further information about acoustic attenuation of optoacoustic waves can be found here [21, 24]. Besides, the bandwidth of ultrasound transducers $F_b(f,z)$ limits the detected frequencies of optoacoustic waves, which are characterized by the phantom measurement described in the following contents. Finally, the simulated frequency $\mathrm{F}(f,z)$ is described [21, 24]:

$$\mathrm{F}(f,z) = F_t(\mathrm{f},\mathrm{z}) \cdot F_a(\mathrm{f},\mathrm{z}) \cdot F_b(\mathrm{f},\mathrm{z}) \quad (3)$$

B. Imaging system

To validate the simulation results, we performed measurements of phantoms and pig esophagus samples using two detectors with different detection bandwidths. Fig. 1(a) shows a schematic of the endoscopy control system, and Fig. 1(b) shows a photograph of the distal end of the optoacoustic endoscopy probe. One detector was a commercially available IVUS transducer (2.5-Fr, Atlantis SR Pro, Boston Scientific, Natick, MA, USA) with a central frequency of 15 MHz and a disc-shaped active element of lead zirconate titanate (PZT) with a diameter of 0.8 mm; the other was a custom-designed IVUS transducer with a central frequency of 50 MHz and a disc-shaped PZT element with a diameter of 0.4 mm. Point-source measurements indicated that the respective acceptance angles of the two detectors were 30 and 40 degrees. Figs. 1(c) and 1(d) indicate the respective simulated sensitivity fields of the two detectors, calculated using the software package Field II [25], which indicate the near field length of both transducers. Samples are usually positioned inside the near-fields in order to enhance the detection sensitivity. The values of near field are calculated at values of 2.5 mm for the 15 MHz detector and 1 mm for the 50 MHz detector based on the simulations.

Light from a 532 nm laser (Wedge HB532, BrightSolutions SRL, Pavia, Italy) with a pulse repetition rate of 2 kHz was delivered via a 400-μm-core multimode side-viewing fiber. Pulse energy was 1 mJ, and pulse width was 0.9 ns. The laser beam was focused and coupled into the fiber through several lenses (Thorlabs), yielding an optical fluence of approximately 12 mJ/cm^2 at the fiber tip. In order to optimize optoacoustic sensitivity over a larger depth range, the side-viewing fiber was aligned such that the laser beam was tilted 15 degrees relative to the ultrasound beam. The two beams began to overlap at near fields of both transducers. The ultrasound detector was connected to a low noise amplifier (63 dB, AU-1291, Miteq, Hauppauge, New York, USA), and amplified signals passed

This article has been accepted for publication in a future issue of this journal, but has not been fully edited. Content may change prior to final publication. Citation information: DOI 10.1109/TMI.2017.2777891, IEEE Transactions on Medical Imaging

through a hybrid rotary joint (Princetel, USA) to a high-speed digitizer operated at 1 GS/s and 12-bit resolution (CS122G1, Gage, Lockport, IL, USA; maximum sampling rate of 2 GS/s). This arrangement reduced noise generated by the rotary joint during rapid rotation. The endoscopy probe was rotated and translated using mechanical stages (Oriental Motor, Japan). Recorded signals were digitally band-pass filtered based on transducer bandwidth, and images were reconstructed using the Hilbert transform.

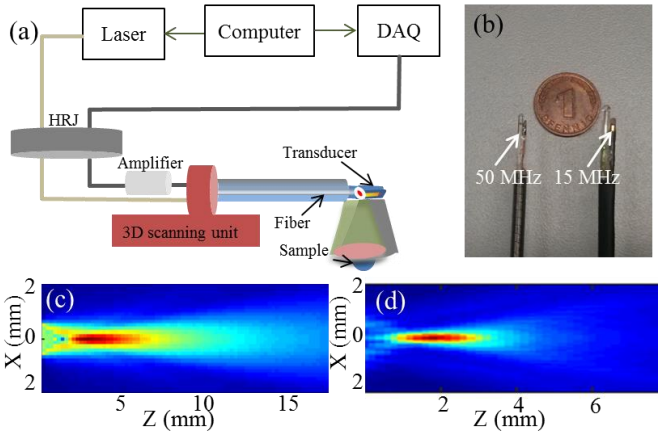

Fig. 1. Schematic of the optoacoustic endoscopy system and simulated sensitivity fields of both transducers. (a) Schematic illustration of the endoscopy set-up. (b) Photograph of the distal end of the two endoscopy probes with central frequencies of 15 or 50 MHz. (c,d) Simulated sensitivity fields of the (c) 15 MHz detector and (d) 50 MHz detector, which indicate the near field length. HRJ: Hybrid Rotary Joint.

C. Phantom and tissue measurements

Bandwidth detection characteristics of the two detectors were determined by scanning a phantom consisting of an agar cylinder containing four 10 µm black polyethylene microspheres positioned at different depths within the agar. The phantom was scanned along the transversal axis. To prevent the detected optoacoustic signals from being affected by variable illumination effects, the excitation laser beam was guided through a fiber bundle and microspheres were fully illuminated. For ex vivo experiments, fresh esophageal sections 6 cm long were obtained from a 1-year-old male pig. The sections were cut open and packed into a polyethylene tube to form a cylindrical structure, as shown in Fig. 5(a). This facilitated imaging the esophageal tissue, since on its own, the sample tended to collapse onto itself. Samples were imaged along several sections using linear or radial scanning using both transducers. Optoacoustic images obtained using the 50 MHz detector were reconstructed using data from three frequency bands (5-20, 20-50 or 50-80 MHz), which were selected using appropriate bandpass filters. The frequency bands were determined based on the simulated frequencies of the main absorbers in different layers of the esophageal wall. Our goal was to investigate the signal frequencies contributed by different layers of the esophageal wall.

III. Results

A. Simulations

Fig. 2 shows the simulated optoacoustic response of an esophageal wall. Fig. 2(a) shows the layer structure with red structures representing blood vessels, which were assumed to be the only optoacoustic absorbers at the excitation wavelength of 532 nm. This simulation predicts that EP and MM layers will be visualized with lower optoacoustic contrast because of the relatively low abundance of vessels, while the LP, SM and MP layers will be visualized with high contrast. Fig. 2(b) shows variations in the simulated blood vessel diameter with increasing depth in the esophageal wall. Fig. 2(c) shows the simulated frequency response of blood vessels with different diameters. The simulation predicts that LP capillaries with an average diameter of 10 µm emit a peak frequency of approximately 150 MHz (at -6 dB), much higher than the peak frequencies of 60 MHz emitted by vessels in the SM layer and of 10-20 MHz emitted by larger vessels in the MP layer.

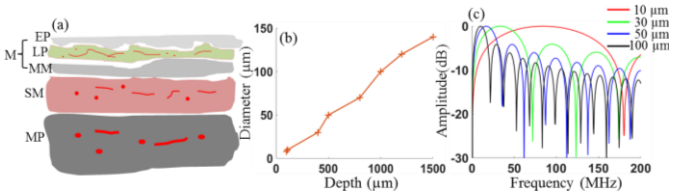

Fig. 2. Simulated frequency response of blood vessels in different layers of the esophageal wall. (a) Layer structure of the superficial esophageal wall. Red structures represent blood vessels. Abbreviations: EP, epithelium; LP, lamina propria; M, mucosa; MM, muscularis mucosa; SM, submucosa; MP, muscularis propria. (b) Diameter of simulated blood vessels with increasing depth in the esophageal wall. (c) Frequency response of simulated blood vessels with diameters of 10-100 µm.

B. Phantom and tissue measurements

Fig. 3 presents characterization results of the microsphere phantom as the distribution of microspheres is illustrated in Fig. 3(a). Figs. 3(b) and 3(c) show optoacoustic images of the microsphere phantom based on data collected using the 15 and 50 MHz detectors, respectively. The ultrasound beams diverge with distance from the probe. SNR values (calculated as the ratio between the highest intensity values and the standard deviation of background) along the depth direction of both transducers are depicted in Fig. 3(c). It can be noted that the SNR values of 15 MHz detector are higher than the values of 50 MHz detector since the larger sensing size of the 15 MHz detectors results in higher sensitivity. Besides, the variations of the lateral and axial resolutions for both detectors quantified with this phantom by FWHM (full width of half maximum) values. The resolution dependencies on the distance between the target and the surface of the probe are plotted in Figs. 3(e) and 3(f), respectively. We can see that the lateral resolutions of both detectors show target distance dependence while the axial resolutions show much less variations. The 50 MHz detector achieves higher resolutions comparing to the 15 MHz detector. For example, the representative lateral and axial resolution values characterized by the first microsphere located approximately 2 mm from the detectors were, respectively, 782 and 186 µm for the 15 MHz transducer and 421 and 69 µm for the 50-MHz transducer.

This article has been accepted for publication in a future issue of this journal, but has not been fully edited. Content may change prior to final publication. Citation information: DOI 10.1109/TMI.2017.2777891, IEEE Transactions on Medical Imaging

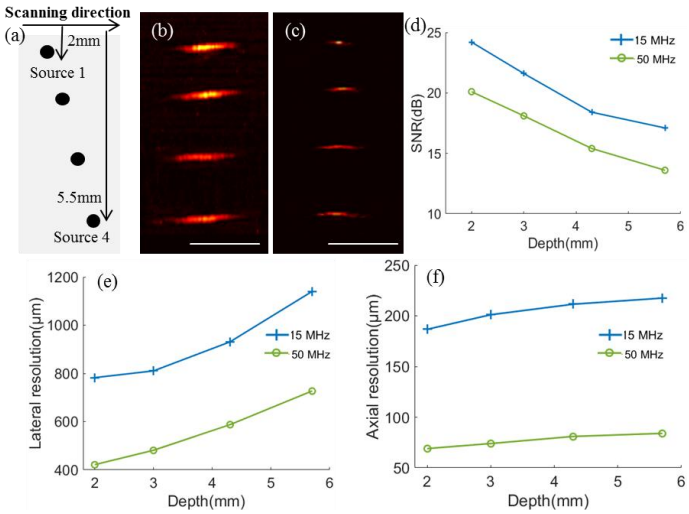

Fig. 3. Optoacoustic imaging of a microsphere phantom using the 15- and 50-MHz transducers. (a) Illustration of the microsphere phantom. (b,c) Images acquired using the (b) 15 MHz or (c) 50 MHz detector. (d) Comparison of the SNR at different depths for the 15 MHz and 50 MHz detectors. (e,f) Lateral and axial resolution along the depth direction for both detectors. Scalebar 1 mm.

To analyze the bandwidth detection characteristics of each detector, we performed a fast Fourier transform of the optoacoustic signals generated by the first microsphere. Fig. 4 shows the optoacoustic signal and corresponding bandwidth for each detector. Pulsewidth is at least 2-fold narrower for the 50 MHz detector comparing to the 15 MHz detector, which explains its higher axial resolution [26]. For the 15-MHz transducer, the central frequency of the spectrum lies at 15 MHz, and bandwidth at −6 dB is 8-22 MHz, corresponding to a fractional bandwidth of 93%. For the 50-MHz transducer, the central frequency lies at 47 MHz, and bandwidth is 26-69 MHz, corresponding to a fractional bandwidth of 85%.

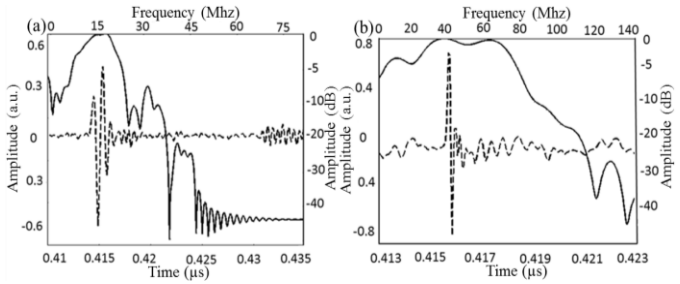

Fig. 4. Bandwidth detection by the 15 and 50 MHz transducers during optoacoustic imaging of a microsphere phantom. (a) Raw optoacoustic signal and the corresponding Fourier-transformed spectrum (dashed line) for the 15 MHz detector. (b) Raw signal and spectrum (dashed line) for the 50 MHz detector.

Next we used the two transducers to image *ex vivo* samples of pig esophagus. Fig. 5(a) shows the orientation of the sample, which was measured along the longitudinal axis as well as in cross-section. Fig. 5(b) shows the layered structure in a longitudinal cross-section of the sample. Figs. 5(c) and 5(d) show optoacoustic images of a longitudinal section corresponding approximately to the position shown in Fig. 5(b). Figs. 5(e) and 5(f) show optoacoustic images of a cross-section from the same sample. The 15 MHz probe achieves penetration depth over 2 mm; however, it does not resolve vessel structures in mucosa well, and it fails to resolve the EP, LP and MM layers. Vascular structures in the SM and MP layers are resolved poorly. The 50 MHz probe, in contrast, resolves vessel structures better, but at shallower depths (approximately 1.5 mm). The 50 MHz probe also resolves the layers of the mucosa better, as indicated by the blue dashed lines in Fig. 5(d). Both transducers reveal clear separation between the mucosa and SM layer, despite the fact that the intervening MM layer comprises several thin layers of smooth muscle fibers, which are expected to show low optoacoustic contrast relative to neighboring tissue.

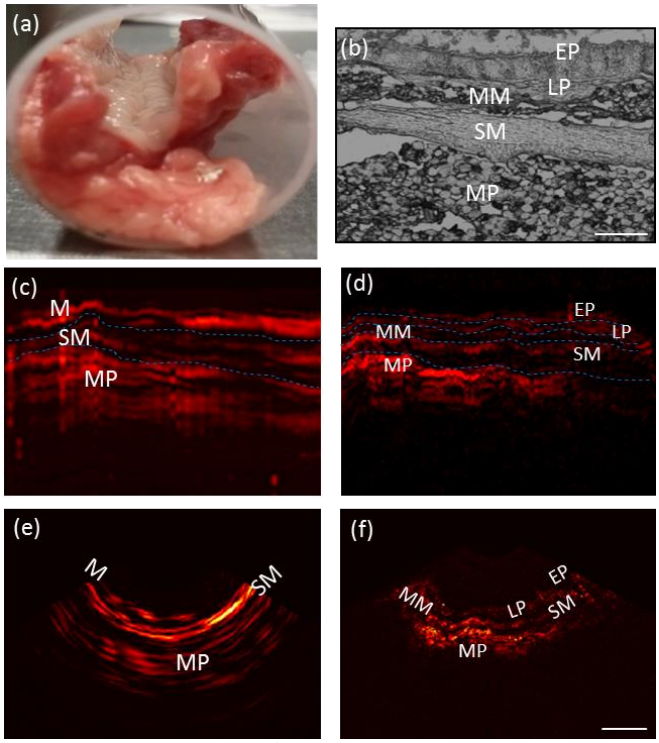

Fig. 5. Optoacoustic imaging of ex vivo pig esophagus using 15 and 50 MHz transducers. (a) Photograph of esophageal tissue in the cylindrical sample holder. (b) Unstained histological image of a longitudinal slice of the sample in (a). (c,d) Optoacoustic images of the same longitudinal slice similar to that in panel (b) generated using data from the (c) 15-MHz detector or (d) 50-MHz detector. Blue dashed lines highlight boundaries between layers. (e,f) Optoacoustic images of the same tissue cross-section generated using data from the (e) 15 MHz detector or (f) 50 MHz detector. Tissue layers are labeled as in Fig. 2(a). Scalebar 500 μm.

Finally we examined which frequency bands in the optoacoustic signal are important for reconstructing the layers of the esophageal wall. Fig. 6 shows optoacoustic image reconstruction of a cross-section of pig esophagus using different frequency bands collected using the 50 MHz detector. Fig. 6(a) shows the image reconstructed using all frequencies in the detection bandwidth. Fig. 6(b) shows the image reconstructed using 5-20 MHz; this image clearly shows the MP layer, while the mucosa and SM layer are less well resolved, and imaging depth does not extend past 1.5 mm. This image is similar to the one in Fig. 5(c), acquired using the full detection bandwidth of the 15 MHz transducer. Fig. 6(c) shows that reconstruction using 20-50 MHz reveals detailed structure in the mucosa and SM layer at depths down to 1 mm. Fig. 6(d) shows the reconstruction using 50-80 MHz, which reveals fine structures, such as capillary dots in the LP layer and vessel edges in the SM layer, albeit to a limited penetration depth of

This article has been accepted for publication in a future issue of this journal, but has not been fully edited. Content may change prior to final publication. Citation information: DOI 10.1109/TMI.2017.2777891, IEEE Transactions on Medical Imaging

only 600 μm. These results indicate that the layer features of the esophageal wall are visualized much better by combining all frequency bands collected by the 50-MHz transducer.

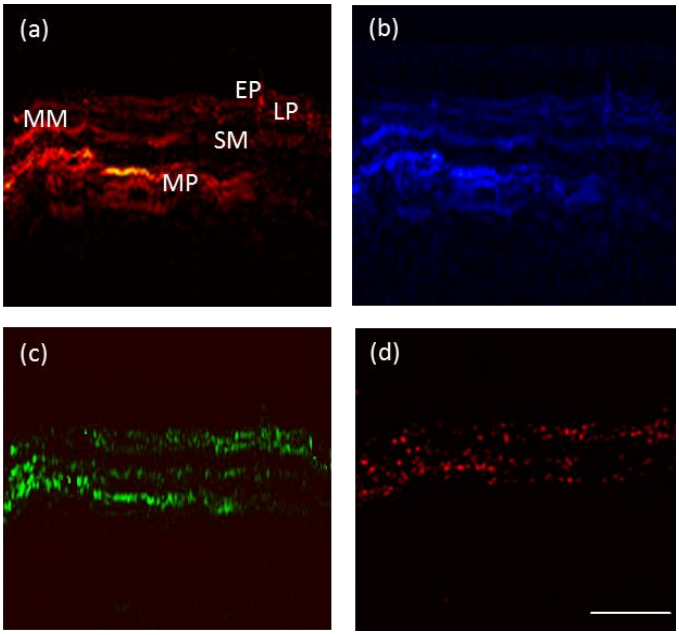

Fig. 6. Frequency bands important for optoacoustic reconstruction of the esophageal wall. The same cross-sectional optoacoustic image was reconstructed using different frequency bands collected with the 50-MHz transducer. (a) Reconstruction based on 5-80 MHz (full detection bandwidth). (b) Reconstruction based on 5-20 MHz. (c) Reconstruction based on 20-50 MHz. (d) Reconstruction based on 50-80 MHz. Scalebar 1 mm.

IV. Discussion

This study examined what optoacoustic detection bandwidth is necessary to reconstruct the layered structure of the esophageal wall. Simulations suggested that a wide frequency band is necessary, and this was confirmed in imaging experiments with ex vivo pig esophagus. In the microsphere phantom measurement, quantitative comparisons in terms of SNR and resolution between the two detectors were investigated, and corresponding results were validated in the pig esophagus measurement. The 50 MHz detector was better than the 15 MHz detector at resolving the LP and SM layers, although the 15 MHz detector was able to image deeper. As we can see in Fig. 5, objects in the SM layer were recovered with blurry by the 15 MHz detector because of its limited resolution, while structures were better visualized in the image of 50 MHz detector since high frequency contents corresponding to the fine structures of the SM layer were recorded. In Fig. 6, optoacoustic signals ranging from 5 to 20 MHz corresponded mainly to gross structure in the MP layer, signals from 20-50 MHz corresponded to finer structure, especially in the LP and SM layers, and signals from 50-80 MHz corresponded to even finer features of the LP and SM layers. Small vessel structures could not be adequately imaged even when detecting the full bandwidth of the 50-MHz detector (5-80 MHz). These results suggest that ultrawide bandwidth detectors ranging from a few MHz to 100 MHz can provide reasonable resolution of esophageal layers.

Our work with phantoms and tissue samples has identified two hardware and software limitations that need to be addressed when developing optoacoustic endoscopic probes. One limitation is the apparent trade-off between the ability to resolve esophageal layers, which was better with the 50 MHz detector in our experiments, and the ability to resolve features deeper within the wall, which was better with the 15 MHz detector. Both abilities are critical for esophageal cancer staging [3, 27, 28]: high-resolution imaging of the esophageal wall allows detailed analysis of the mucosa and SM layer, which is important for detecting esophageal cancer in earlier stages; deeper imaging offers the possibility of detecting more advanced lesions that have invaded into the wall [4, 29]. The development of accurate optoacoustic endoscopes will require optimizing this trade-off. A good solution may be an ultrawide bandwidth transducer covering the bandwidths of the 15 and 50 MHz detectors or an even wider bandwidth. Such transducers are commercially available, but they are too large for endoscopy applications.

The second limitation identified in our work is the finite aperture effect of the detector, which led to relatively low lateral resolution in our reconstructed images. For IVUS detectors, the lateral resolution is mainly determined by the size of the sensing area. Although it may be possible to improve this resolution using more advanced reconstruction methods, this is likely to be extremely challenging in the case of endoscopy imaging [30]. A potentially more feasible option is to use focused ultrasound detectors that can provide high-resolution images at the focus [11, 19].

The present study makes clear that ultrawide bandwidth transducers are necessary for optoacoustic endoscopy capable of resolving the layers of the esophageal wall. It further suggests the need to strike a reasonable balance between resolution and imaging depth in order to permit accurate early staging of esophageal cancer. Since excised samples contain different absorption properties comparing to live tissue, more human esophageal samples and in vivo including health and diseased ones should be measured to further investigate the necessary optoacoustic detection properties for future esophageal imaging. Overall, the present work may help guide the design of optoacoustic endoscopes that are more accurate than ultrasound and provide more clinically useful information than confocal or OCT.

Acknowledgment

We thank Dr. Chapin Rodriguez for his attentive reading and improvements of the manuscript. We thank Dr. habil. Krzysztof Flisikowski for providing the pig esophagus samples. Xiaohua Jian and Yaoyao Cui designed and fabricated the 50 MHz ultrasound transducer.

References

[1] M. Vieth, C. Ell, L. Gossner, A. May, and M. Stolte, "Histological Analysis of Endoscopic Resection Specimens From 326 Patients with Barrett's Esophagus and Early Neoplasia," *Endoscopy*, vol. 36, pp. 776-781, 24.08.2004 2004.

[2] B. J. Reid, P. L. Blount, and P. S. Rabinovitch, "Biomarkers in Barrett's esophagus," *Gastrointest Endosc Clin N Am*, vol. 13, pp. 369-397, 4 2003.

[3] M. F. Berry, "Esophageal cancer: staging system and guidelines for staging and treatment," *J Thorac Dis*, vol. 6 Suppl 3, pp. S289-97, May 2014.

[4] S.-R. Puli, "Staging accuracy of esophageal cancer by endoscopic ultrasound: A meta-analysis and systematic review," *World Journal of Gastroenterology*, vol. 14, p. 1479, 2008.

[5] J. Mannath and K. Ragunath, "Role of endoscopy in early oesophageal cancer," *Nat Rev Gastroenterol Hepatol*, Nov 03 2016.

[6] T. Attila and D. O. Faigel, "Role of endoscopic ultrasound in superficial esophageal cancer," *Dis Esophagus*, vol. 22, pp. 104-12, 2009.

[7] A. T. Committee, V. Kaul, D. G. Adler, J. D. Conway, F. A. Farraye, S. V. Kantsevoy, *et al.*, "Interventional EUS," *Gastrointest Endosc*, vol. 72, pp. 1-4, Jul 2010.

[8] P.-A. Testoni, "Optical coherence tomography in detection of dysplasia and cancer of the gastrointestinal tract and bilio-pancreatic ductal system," *World Journal of Gastroenterology*, vol. 14, p. 6444, 2008.

[9] B. J. Vakoc, D. Fukumura, R. K. Jain, and B. E. Bouma, "Cancer imaging by optical coherence tomography: preclinical progress and clinical potential," *Nat Rev Cancer*, vol. 12, pp. 363-8, May 2012.

[10] G. D. De Palma, "Confocal laser endomicroscopy in the "in vivo" histological diagnosis of the gastrointestinal tract," *World Journal of Gastroenterology*, vol. 15, p. 5770, 2009.

[11] J. M. Yang, C. Favazza, R. Chen, J. Yao, X. Cai, K. Maslov, *et al.*, "Simultaneous functional photoacoustic and ultrasonic endoscopy of internal organs in vivo," *Nat Med*, vol. 18, pp. 1297-1302, Aug 2012.

[12] H. He, A. Buehler, and V. Ntziachristos, "Optoacoustic endoscopy with curved scanning," *Opt Lett*, vol. 40, pp. 4667-70, Oct 15 2015.

[13] H. He, G. Wissmeyer, S. V. Ovsepian, A. Buehler, and V. Ntziachristos, "Hybrid optical and acoustic resolution optoacoustic endoscopy," *Opt Lett*, vol. 41, pp. 2708-10, Jun 15 2016.

[14] V. Ntziachristos, "Going deeper than microscopy: the optical imaging frontier in biology," *Nat Methods*, vol. 7, pp. 603-14, Aug 2010.

[15] A. Taruttis and V. Ntziachristos, "Advances in real-time multispectral optoacoustic imaging and its applications," *Nature Photonics*, vol. 9, pp. 219-227, 2015.

[16] D. Razansky, M. Distel, C. Vinegoni, R. Ma, N. Perrimon, R. W. Köster, *et al.*, "Multispectral opto-acoustic tomography of deep-seated fluorescent proteins in vivo," *Nature Photonics*, vol. 3, pp. 412-417, 2009.

[17] A. Taruttis, G. M. van Dam, and V. Ntziachristos, "Mesoscopic and Macroscopic Optoacoustic Imaging of Cancer," *Cancer Res*, vol. 75, pp. 1548-1559, Apr 15 2015.

[18] J. M. Yang, K. Maslov, H. C. Yang, Q. Zhou, K. K. Shung, and L. V. Wang, "Photoacoustic endoscopy," *Opt Lett*, vol. 34, pp. 1591-3, May 15 2009.

[19] J. M. Yang, R. Chen, C. Favazza, J. Yao, C. Li, Z. Hu, *et al.*, "A 2.5-mm diameter probe for photoacoustic and ultrasonic endoscopy," *Opt Express*, vol. 20, pp. 23944-53, Oct 8 2012.

[20] J. Aguirre, M. Schwarz, N. Garzorz, M. Omar, A. Buehler, K. Eyerich, *et al.*, "Precision assessment of label-free psoriasis biomarkers with ultra-broadband optoacoustic mesoscopy," *Nature Biomedical Engineering*, vol. 1, p. 0068, 2017.

[21] M. Schwarz, D. Soliman, M. Omar, A. Buehler, S. V. Ovsepian, J. Aguirre, *et al.*, "Optoacoustic Dermoscopy of the Human Skin: Tuning Excitation Energy for Optimal Detection Bandwidth With Fast and Deep Imaging in vivo," *IEEE Trans Med Imaging*, vol. 36, pp. 1287-1296, Jun 2017.

[22] A. L. K. a. L. L.Tres, *Histology and Cell Biology: An Introduction to Pathology*, 3 ed.: Elsevier / Mosby; , 2011.

[23] M. H. Xu and L. H. V. Wang, "Photoacoustic imaging in biomedicine," *Review of Scientific Instruments*, vol. 77, p. 041101, Apr 2006.

[24] X. L. Dean-Ben, D. Razansky, and V. Ntziachristos, "The effects of acoustic attenuation in optoacoustic signals," *Phys Med Biol*, vol. 56, pp. 6129-48, Sep 21 2011.

[25] J. A. Jensen, "Field: A Program for Simulating Ultrasound Systems," *Medical & Biological Engineering & Computing*, vol. 34, pp. 351-353, 1996.

[26] M. Xu and L. Wang, "Analytic explanation of spatial resolution related to bandwidth and detector aperture size in thermoacoustic or photoacoustic reconstruction," *Physical Review E*, vol. 67, 2003.

[27] L. J. He, H. B. Shan, G. Y. Luo, Y. Li, R. Zhang, X. Y. Gao, *et al.*, "Endoscopic ultrasonography for staging of T1a and T1b esophageal squamous cell carcinoma," *World J Gastroenterol*, vol. 20, pp. 1340-7, Feb 7 2014.

[28] G. Sgourakis, I. Gockel, and H. Lang, "Endoscopic and surgical resection of T1a/T1b esophageal neoplasms: a systematic review," *World J Gastroenterol*, vol. 19, pp. 1424-37, Mar 7 2013.

[29] V. Conteduca, D. Sansonno, G. Ingravallo, S. Marangi, S. Russi, G. Lauletta, *et al.*, "Barrett's esophagus and esophageal cancer: An overview," *International Journal of Oncology*, vol. 41, pp. 414-424, Aug 2012.

[30] Y. L. Sheu, C. Y. Chou, B. Y. Hsieh, and P. C. Li, "Image reconstruction in intravascular photoacoustic imaging," *IEEE Trans Ultrason Ferroelectr Freq Control*, vol. 58, pp. 2067-77, Oct 2011.